Available online at www.sciencedirect.com
SCIENCE DIRECT
Talanta 68 (2005) 429–436
Talanta
www.elsevier.com/locate/talanta

# Microfluidic cells with interdigitated array gold electrodes: Fabrication and electrochemical characterization

Daniela Daniel, Ivano G.R. Gutz *

*Instituto de Química, Universidade de São Paulo, Av. Prof. Lineu Prestes, 748, 05508-000 São Paulo, Brazil*

Received 16 July 2005; received in revised form 3 September 2005; accepted 3 September 2005

**Abstract**

Microfluidic flow cells combined with an interdigitated array (IDA) electrode and/or individually driven interdigitated electrodes were fabricated and characterized for application as detectors for flow injection analysis. The gold electrodes were produced by a process involving heat transfer of a toner mask onto the gold surface of a CD-R and etching of the toner-free gold region by short exposure to iodine-iodide solution. The arrays of electrodes with individual area of 0.01 $cm^2$ (0.10 cm of length × 0.10 cm of width and separated by gaps of 0.05 or 0.03 cm) were assembled in microfluidic flow cells with 13 or 19 μm channel depth. The electrochemical characterization of the cells was made by voltammetry under stationary conditions and the influence of experimental parameters related to geometry of the channels and electrodes were studied by using $K_4Fe(CN)_6$ as model system. The obtained results for peaks currents ($I_p$) are in excellent agreement with the expected ones for a reversible redox system under stationary thin-layer conditions. Two different configurations of the working electrodes, $E_i$, auxiliary electrode, *A*, and reference electrode, *R*, on the chip were examined: $E_i/R/A$ and $R/E_i/A$, with the first presenting certain uncompensated resistance. This is because the potentiostat actively compensates the *iR* drop occurring in the electrolyte thin layer between *A* and *R*, but not from *R* to each $E_i$. This is confirmed by the smaller difference between the cathodic and anodic peak potentials for the second configuration. Evaluation of the microfluidic flow cells combined with (individually driven) interdigitated array electrodes as biamperometric or amperometric detectors for FIA reveals stable and reproducible operation, with peak heights presenting relative standard deviations of less than 2.2%. For electrochemically reversible species, FIA peaks with enhanced current signal were obtained due to *redox cycling* under flow operation. The versatility of microfluidic flow cells, produced by simple and low-cost technique, associated with the rich information content of electrochemical techniques with arrays of electrodes, opens many future research and application opportunities.


*Keywords:* Interdigitated array (IDA) electrodes; Gold electrodes; Microfluidic flow cell; Cyclic voltammetry; Amperometry; Biamperometry; FIA

## 1. Introduction

The recent trend to miniaturize chemical assays is stimulating the development of the field of microfluidic devices. The small scale of the experiments result in amazing reduction in solution consumption, meaning that lower volumes of sample and reagents are required and less waste is generated. Improved fabrication techniques and the use of new materials are helping the field to move toward its ultimate goal of producing functional and low-cost micro total analysis systems (μTAS) [1]. Electrochemical detectors are an attractive alternative in microfluidics [2,3] because most techniques are interfacial ones (compatible with thin layer operation and small sample volumes) and provide low detection limits. The placement of electrochemical detectors in microchannels' demands microfabrication technologies and is being extensively investigated because of its expected great potential for chemical analysis especially when coupled with separation methods and integrated in μTAS [4–7].

Strategies for increasing sensitivity and minimizing interferences comprise the use of multiple electrode configurations [8,9], such as individually driven interdigitated electrodes [10]. Electrochemical sensors with dual electrodes show enhanced sensitivity over single electrode ones [4,5]. Dual (or multiple) electrodes can be placed in the channels in a series configuration [9,11], thus forcing solutions to flow across one electrode before the next electrode, a condition that presents similarity with ring-disk experiments. By setting the potentials accordingly, the upstream electrode can either electrochemically generate electroactive species or eliminate interferents that are electroactive at lower potentials than the analyte(s), so that the downstream

* Corresponding author. Tel.: +55 11 3091 2150; fax: +55 11 3091 2150.
*E-mail address:* gutz@iq.usp.br (I.G.R. Gutz).

0039-9140/$ – see front matter © 2005 Elsevier B.V. All rights reserved.
doi:10.1016/j.talanta.2005.09.003

electrode acts as a collector or is screened, leading to more selective detection [11–13].

Interdigitated array (IDA) electrodes have been used as highly sensitive detectors because of their inherent features, such as large currents, high sensitivity, and rapid current rise to a steady state. Niwa and co-workers [14] have pioneered this technique for the electrochemical amplification of reversible redox species. The redox species electrogenerated at one band electrode (generator) of an IDA diffuses to adjacent band electrodes (collector), where it is regenerated to its original state. This so-called *redox cycling* process greatly enhances the current signal because when the potentials of the band electrodes are adjusted to promote the consecutive oxidation and reduction, the same molecule can react many times along its path through the cell.

Theoretically, the current at the electrode in a thin layer flow cell is proportional to the cube root of the flow rate [15]. This is because the diffusion layer thickness increases when the flow rate is decreased. By contrast, the redox species signal at the IDA electrodes doesnot decrease by reducing the flow rate in the low flow rate region because the effect of the diffusion layer formed between two band electrodes in the IDA becomes dominant and the diffusion layer thickness is not significantly influenced by the flow rate. In other words, the flow rate of redox cycling for IDA detection is constant in the amperometric region and depends only on the IDA dimensions [14]. This fact reveals that effective electrochemical detection with interdigitated array electrodes in microfluidic flow cells can be advantageous for reversible redox systems and deserves wider exploration in analytical applications.

Although array electrodes have found many practical applications [16–18], such as in flow analysis [19–21], the manufacture of IDA is not straightforward and is difficult to implement in the electroanalytical laboratory where microphotolithographic techniques are usually not available [10,22–24]. Recently, simpler approaches to produce microchannels, based on thermal transfer of laser-printed toner masks and spacers, have been invented [25,26], with great potentiality in most applications where the sub-micrometric resolution of the microphotolithography is not required. The attractiveness of this alternative is that the complex manufacturing technology of microfluidic devices in the clean room is substituted by procedures and resources available in any analytical laboratory.

In this paper, studies carried out with microfluidic cells produced by the thermal transfer of laser-printed toner masks on gold CD-Rs are presented. The electrochemical performance of these cells was evaluated under thin-layer conditions for individual band electrodes or groups of interdigitated electrodes, at two heights of the microchannel (∼13 μm, obtained by stacking two layers of toner and ∼19 μm, given by three layers) and two different positions of the reference electrode in relation to the working electrodes, under both stationary and flow operation. The microfluidic cell with IDA gold electrodes was examined as a biamperometric or amperometric detector for FIA. Additionally, amperometric measurements with the IDA having one comb as working electrode and the other one as auxiliary electrode were compared with one comb as working electrode and an external auxiliary electrode.

## 2. Experimental

### 2.1. Fabrication of microfluidic cells with integrated IDA gold electrodes

The fabrication process described in a previous paper [26] and summarized here was used to manufacture the microfluidic flow cell with integrated IDA gold electrodes. The first step is to draw the image of the desired electrode's layout on a 1:1 scale, using any drawing software. This image is laser printed on wax paper and the toner mask is heat transferred onto the gold surface of a slice of a proper CD-R (Mitsui Gold), after removal of the protective polymer layer. The toner-free gold regions are etched by exposure to an iodide/iodine solution. Afterwards, the toner mask is removed with acetonitrile. A further step consisted in integrating these electrodes into a microfluidic flow cell. The CD slice with the printed electrodes is heat bonded with another polycarbonate slice by a toner layer acting as spacer and gasket. A channel obtained with one layer of toner presents a depth of nearly 7 μm; by overlaying two toner masks (sequential thermal transfer), the channel steps to 13 μm, and so forth. Microfluidic flow cells with channel-depths of approximately 13 or 19 μm (relative to the unprinted areas) were constructed by piling up two or three toner layers, respectively.

Sketches of the construction of the microflow cells are shown in Fig. 1. Various combinations are possible for the use of the gold band electrodes in these cells: single band or multiple band electrodes can be controlled against external reference and auxiliary electrodes for voltammetry or amperometric detection; a downstream band can act as an internal auxiliary electrode of an upstream working band; or generator–collector series can be setup with the interdigitated combs. The last alternative may constitute a low-cost replacement for ring-disk electrodes [27]. The tip of a miniaturized reference electrode [28] was pressure fitted to orifices in the upper part of the cell. An external auxiliary electrode, for comparison purposes with the internal one, was placed at the cell outlet (a stainless steel tube serving both purposes).

The overall internal volume of cell shown in Fig. 1B was estimated to be 182 or 266 nl, for double or triple toner layers, respectively. The geometrical volume of the channel above each rectangular band electrode (with 0.10 cm width) corresponds to approximately 13 or 19 nl for double or triple toner layers, respectively. The IDA gold electrode consisted of pairs of 0.100-cm electrodes separated by gaps of 0.030 cm, the spacing gap used for individually driven interdigitated gold electrodes was 0.050 cm. The hydrodynamic flow regime along the working electrode(s) is assumed to be laminar, on account of the reduced channel size (1.4 cm of length × 0.1 cm of width × 13 or 19 μm of height) and the relatively low fluid velocity (some cm $s^{-1}$), rendering a low Reynolds number.

### 2.2. Materials and reagents

All solid reagents were of analytical grade and were used without further purification. Solutions were prepared by dis-

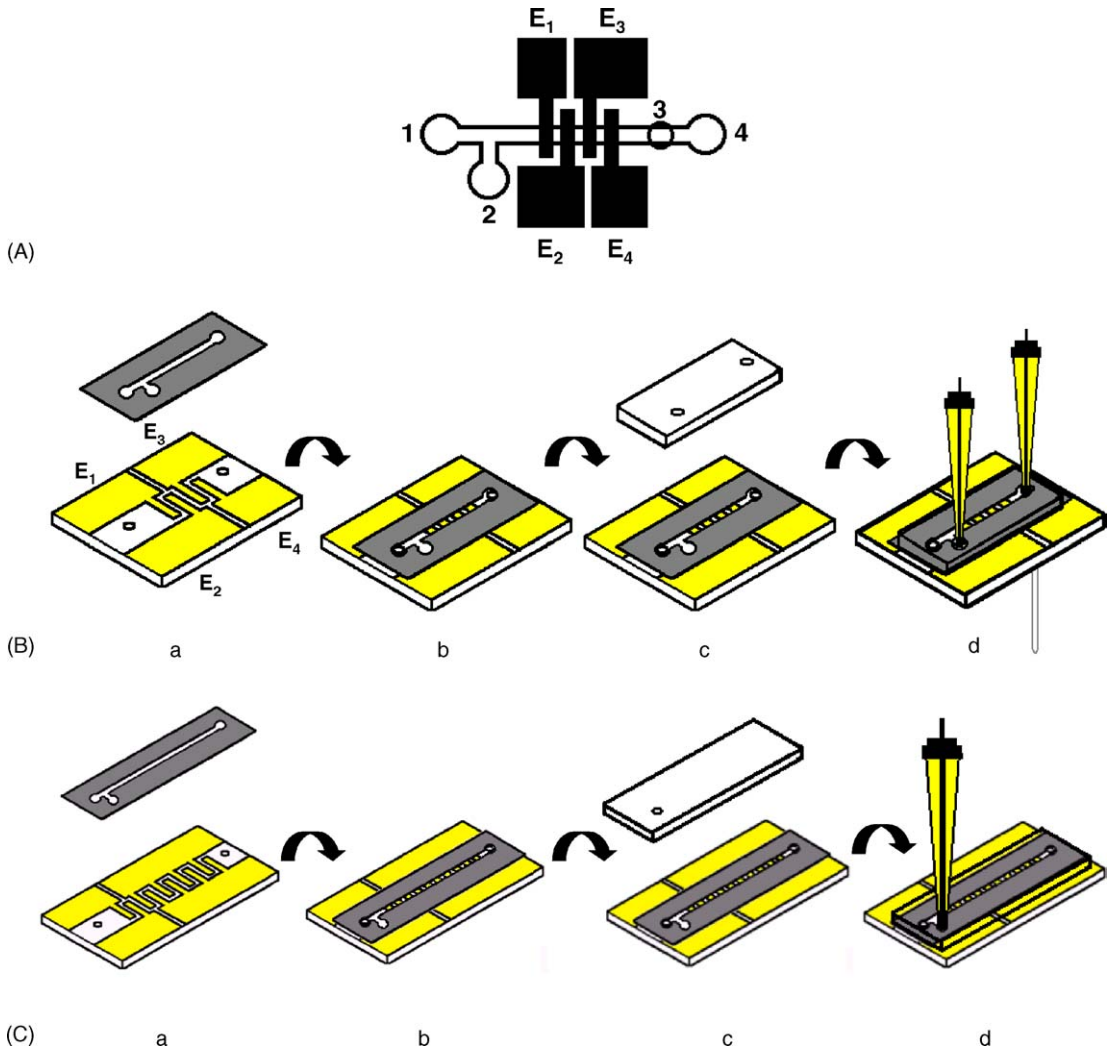


Fig. 1. Sketches of the construction of individually driven interdigitated gold electrodes and IDA gold electrodes assembled into microfluidic cells. (A) Top schematic view of the microfluidic device. (1) Inlet; (2) reference electrode, located next to inlet to the cell; (3) reference electrode, located next to outlet to the cell; (4) outlet and auxiliary electrode; ($E_{1–4}$) working electrodes. (B) Schematic illustration of the construction of a microfluidic cell with four individually driven gold electrodes. (a) Polycarbonate slice with finished Au working electrodes ($E_1$–$E_4$) and orifices for flow inlet and outlet, and toner mask of channels (wax paper not shown) before application; (b) same components of (a) after heat-transfer of toner channel; (c) microfluidic flow cell before heat-sealing of the second polycarbonate slice; (d) complete microfluidic cell with two attached miniaturized Ag/AgCl reference electrodes (only one required for normal operation). (C) Schematic illustration of the construction of a microfluidic cell with IDA of electrodes and two extra electrodes. (a), (b) and (c), description similar to (B); (d) complete IDA microfluidic cell with attached miniaturized Ag/AgCl reference electrode.

solving the reagents in deionized water (18 MΩ cm) processed through a water purification system (Nanopure UV, Barnstead, Dubuque, IA). Analyte solutions were prepared daily by dissolving potassium ferrocyanide ($K_4Fe(CN)_6$) and potassium chloride (KCl) in deionized water.

All electrochemical experiments were performed at room temperature with a homemade potentiostat based on operational amplifiers connected to an interface card (PCL711B) with 12 bits A/D and D/A converters and digital control lines, placed in a slot of a personal computer. The software, written in Delphi language, controls the applied potentials and scan rates and executes data acquisition of current measurements, previously converted in proportional voltages by an operational amplifier with gain control. Cyclic voltammetry was performed under stationary conditions using a miniaturized Ag/AgCl reference electrode [28] and a stainless steel tube as auxiliary electrode. For amperometric measurements, the solutions were introduced into the microfluidic flow cell by a peristaltic pump (MS Reglo, Ismatec, Zurich, Switzerland) fitted with narrow bore tubing (i.d. = 0.25 mm) and a pneumatic damper. Pulsation interference increases at lower rpm, hindering work at flow rates below 120 μl $min^{-1}$. For FIA experiments, a manual, narrow bore rotary valve injector was inserted between the pump and the cell; sample volumes of 3 or 10 μl were used, as given in the figure captions. The flow rate and injection volume settings had not been optimized and lower settings of both should be considered in future work.

## 3. Results and discussion

### *3.1. Individually driven gold strip electrodes characterization under thin layer conditions*

The characteristics of cyclic voltammetry with microelectrodes in a microchannel have been discussed in the literature [29,30]. However, there are few reports about the electrochemical properties of systems with multiple electrodes in microfluidic channels [7], with little or no discussion about the effects of geometric factors, like depth of the microchannel, distance and positioning of the working electrodes in relation to reference and auxiliary electrodes, on the electrochemical performance cells [31]. A difficulty for electrochemical measurements in low depth channels is the low conductance of the thin layer of electrolyte. When the reference and auxiliary electrodes are placed outside the thin-layer chamber and the electrolyte/analyte ratio is not high enough, for relatively "large" working electrodes compared to the channel section, one can have severe non-uniformity of the potential on its surface as well as high-uncompensated *iR* drops, producing for example, non-linear potential sweeps and distorted voltammograms.

The oxidation of the potassium ferrocyanide was used to test the electrochemical response of the cell under finite diffusion conditions (with the microfluidic flow cell shown in Fig. 1B). Fig. 2A presents cyclic voltammograms obtained scanning at $10\,\mathrm{mV\,s^{-1}}$ between 0.1 and 0.4 V in the presence of $1.17 \times 10^{-3}\,\mathrm{mol\,l^{-1}}$ $K_4Fe(CN)_6$ in $0.2\,\mathrm{mol\,l^{-1}}$ KCl for a thin-layer with 13 μm of thickness at stationary condition, for each of four individually driven interdigitated gold electrodes ($E_1$–$E_4$). For this data, the reference electrode, *R*, is located between the working electrode, $E_i$, and auxiliary electrode, *A*, as depicted in Fig. 1A. This configuration will be referred as $E_i/R/A$ now on. Fig. 2B shows cyclic voltammograms for the same set of electrodes under identical conditions, but with the reference electrode close to the inlet of the microfluidic cell, in a $R/E_i/A$ configuration (Fig. 1A). Fig. 3 was obtained for a channel depth of 19 μm, in the $E_i/R/A$ configuration (Fig. 3A) and the $R/E_i/A$ configuration (Fig. 3B).

The results for this series of experiments were gathered in Table 1. By switching from the $R/E_i/A$ to the $E_i/R/A$ configuration, the difference between the cathodic and anodic peak potentials increases from 0.015 to 0.046 V for $E_1$. This is expected because in the second configuration the misplacing of the reference electrode hinders the potentiostat from compensating the *iR* drop in the electrolyte thin layer between the tip of *R* and the working electrode(s). In fact, by switching sequentially from electrodes $E_4$ to $E_1$ in the second configuration, the $\Delta E_p$ increases, while it is rather unaffected in the $R/E_i/A$ setup. When various $E_i$ are connected simultaneously, in the $E_i/R/A$ setup the *iR* drop becomes more significant from $E_4$ to $E_1$, while in the $R/E_i/A$ configuration, $E_1$ will be correctly potentiostated, while some overcompensation will be noticed for $E_2$–$E_4$, growing in this order.

By increasing the channel depth to three layers of toner (∼19 μm) and keeping the electrolyte/analyte ratio at the same ratio of 170 used before, lower $\Delta E_p$ values were observed due

Table 1
Cyclic voltammetry data for experiments with individually interdigitated gold electrodes in microfluidic cells for two and three toner layer at different positions of the reference electrode

| | Two toner layers cell (∼13 μm) | | | | | | | Three toner layers cell (∼19 μm) | | | | | | |
|---|---|---|---|---|---|---|---|---|---|---|---|---|---|---|
| | Electrodes configuration $R/E_1$–$E_4/A$ | | | | Electrodes configuration $E_1$–$E_4/R/A$ | | | Electrodes configuration $R/E_1$–$E_4/A$ | | | | Electrodes configuration $E_1$–$E_4/R/A$ | | |
| | $I_{pa}$ | $I_{pc}$ | $\Delta E_p$ | $E^{0'}$ | $I_{pa}$ | $I_{pc}$ | $\Delta E_p$ | $E^{0'}$ | $I_{pa}$ | $I_{pc}$ | $\Delta E_p$ | $E^{0'}$ | $I_{pa}$ | $I_{pc}$ | $\Delta E_p$ | $E^{0'}$ |
| $E_1$ | 0.132 | −0.096 | 0.015 | 0.270 | 0.124 | −0.100 | 0.046 | 0.279 | 0.201 | −0.162 | 0.005 | 0.276 | 0.197 | −0.160 | 0.025 | 0.278 |
| $E_2$ | 0.126 | −0.100 | 0.014 | 0.272 | 0.113 | −0.093 | 0.033 | 0.278 | 0.188 | −0.160 | 0.008 | 0.277 | 0.196 | −0.150 | 0.025 | 0.277 |
| $E_3$ | 0.126 | −0.093 | 0.009 | 0.271 | 0.123 | −0.090 | 0.026 | 0.283 | 0.189 | −0.160 | 0.008 | 0.277 | 0.199 | −0.158 | 0.025 | 0.279 |
| $E_4$ | 0.120 | −0.090 | 0.010 | 0.271 | 0.112 | −0.086 | 0.025 | 0.283 | 0.191 | −0.159 | 0.008 | 0.277 | 0.193 | −0.152 | 0.020 | 0.278 |

Concentration: $1.17 \times 10^{-3}\,\mathrm{mol\,l^{-1}}$ of $K_4Fe(CN)_6$ solution in $0.2\,\mathrm{mol\,l^{-1}}$ KCl. Scan rate: $10.0\,\mathrm{mV\,s^{-1}}$. $E_{1\text{–}4}$: working electrodes (see Fig. 1A); *R*: reference electrode; *A*: auxiliary electrode; $I_{pa}$: anodic current peak (μA); $I_{pc}$: cathodic current peak (μA); $\Delta E_p$: separation of cathodic and anodic peaks (V); $E^{0'}$: formal redox potential (V).

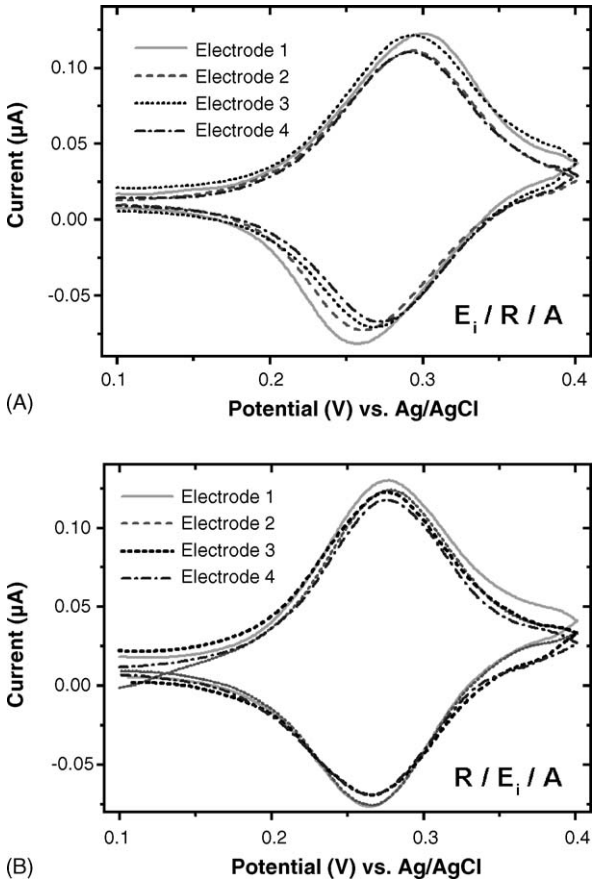


Fig. 2. Cyclic voltammograms of a $1.17 \times 10^{-3}$ mol l$^{-1}$ $K_4Fe(CN)_6$ solution in KCl 0.2 mol l$^{-1}$ for four individually driven interdigitated gold electrodes in microfluidic cell with 13 μm deep channel. Potential scan rate: 10.0 mV s$^{-1}$. (A) $E_i/R/A$ configuration and (B) same set electrodes of "A" using $R/E_i/A$.

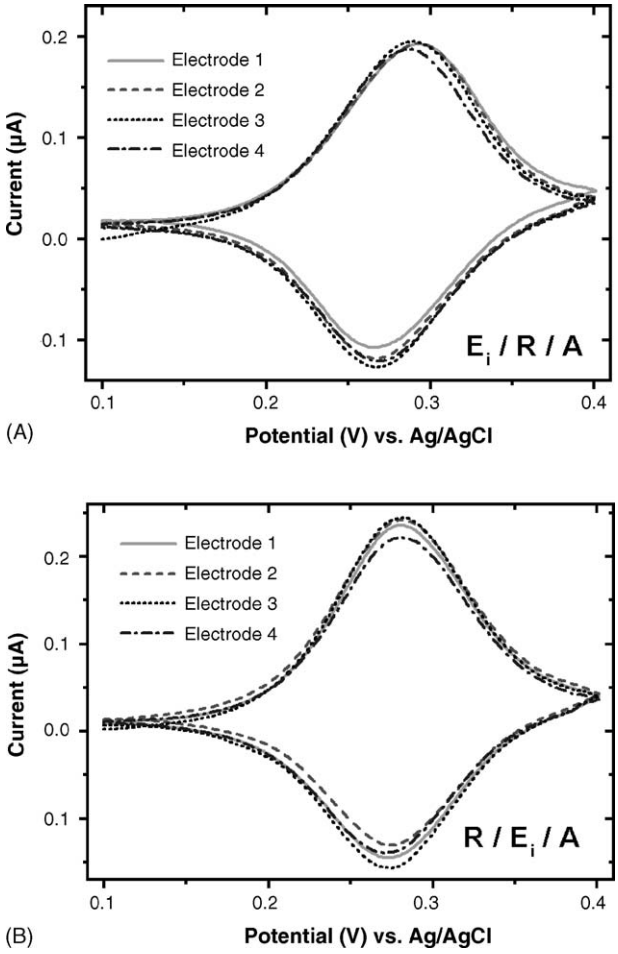


Fig. 3. Cyclic voltammograms obtained in microfluidic cell with 19 μm deep channel. Same conditions of Fig. 2.

to the thicker layer of conducting electrolytic, e.g., of 0.005 and 0.025 V for $E_1$, respectively, in $R/E_i/A$ and $E_i/R/A$ configurations. The formal redox potentials, calculated from the average of the cathodic ($E_{pc}$) and anodic ($E_{pa}$) peak potentials, $E^{0'} = (E_{pc} + E_{pa})/2$, are very close to the literature value [32], in all cases.

A theoretical treatment of current–voltage curves for a reversible redox system under stationary thin-layer conditions was presented by Hubbard [34]. The peak is symmetrical and the peak current is linearly related to the scan rate according to the equation [33]:

$$i_p = n^2 F^2 (4RT)^{-1} A d C_o^* \nu \quad (1)$$

where, $n$ is the number of electrons transferred, $F$ the Faraday constant (96 485 C mol$^{-1}$), $R$ the universal gas constant, $T$ the absolute temperature, $A$ the area of the electrode (cm$^2$), $d$ the thickness of the solution layer (cm), $C_o^*$ the concentration (mol cm$^{-3}$) of the analyte in the bulk solution and $\nu$ is the scan rate (V s$^{-1}$). For an ideal Nernstian behavior, there is no difference between the cathodic and anodic peak potentials, $[E_{pa} - E_{pc}] = 0$, and the peak current is directly proportional to $\nu$. From Eq. (1), the current values were calculated as 0.143 and 0.208 μA, for two and three toner layers, respectively. In contrast, the average of experimental values were 0.122 and 0.194 μA for microfluidic cell with a channel-depth of about 13 and 19 μm, respectively. The small difference between the expected and found value might be caused by the uncertainty in the channel depths and some contribution of radial diffusion at the electrode edges.

In a different approach, data from Figs. 2B and 3B was used to obtain the charge involved in the anodic and cathodic peaks (integration with background correction); by calculating the volume of solution that contains the number of moles of ferrocyanide involved in the oxidation/reduction cycle, the values of 13.5 and 18.7 nl were obtained for the thin layer above electrode, again, very close to the estimated geometrical ones, of 13 and 19 nl.

The effect of the $K_4Fe(CN)_6$ concentration on the cyclic voltammograms was evaluated, looking for analytical applications of the microfluidic cell in the $R/E_i/A$ configuration. A linear calibration curve was defined for the explored region of $1.17 \times 10^{-5}$ mol l$^{-1}$–$1.17 \times 10^{-3}$ mol l$^{-1}$, with a correlation coefficient of 0.999. The detection limit for $K_4Fe(CN)_6$ calculated as three times the standard deviation of the blank ($3\sigma$) was $2.8 \times 10^{-6}$ mol l$^{-1}$. As expected, in the examined region of 5–20 m V s$^{-1}$, a linear dependence of scan rate of the cyclic voltammograms and peak height was observed.

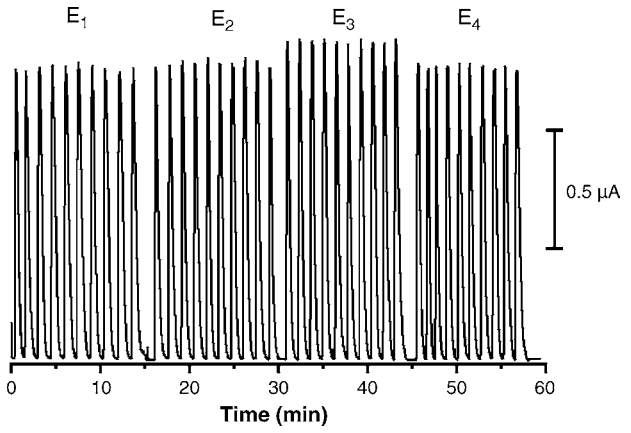


Fig. 4. Amperometric response for four individually driven interdigitated gold electrodes in microfluidic flow cell with 19 μm deep channel. Injections of 3 μl of $1.17 \times 10^{-3}$ mol l$^{-1}$ $K_4Fe(CN)_6$ solution in KCl 0.2 mol l$^{-1}$, at 100 μl min$^{-1}$ and 0.400 V vs. Ag/AgCl applied potential. Average currents at the electrodes (in μA): ($E_1$) $1.23 \pm 0.01$ (RSD = 0.8%); ($E_2$) $1.26 \pm 0.01$ (RSD = 0.8%); ($E_3$) $1.35 \pm 0.02$ (RSD = 1.5%); ($E_4$) $1.24 \pm 0.01$ (RSD = 0.8%).

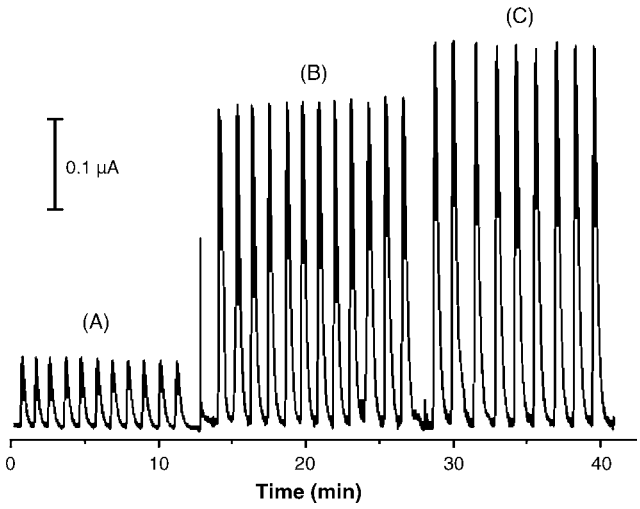


Fig. 5. Amperometric response for 10-μl injections of $1.17 \times 10^{-4}$ mol l$^{-1}$ $K_4Fe(CN)_6$ in 0.2 mol l$^{-1}$ KCl, at 150 μl min$^{-1}$ and 0.400 V vs. Ag/AgCl applied potential. (A) One electrode band. Average current: $0.091 \pm 0.002$ μA (RSD = 2.2%); (B) a comb with four bands' electrode and external auxiliary electrode. Average current: $0.386 \pm 0.004$ μA (RSD = 1.1%). (C) Same comb of "A" using other equivalent comb as internal auxiliary electrode. Average current: $0.444 \pm 0.005$ μA (RSD = 1.1%).

### 3.2. Flow injection studies of the individually driven interdigitated gold electrodes

Flow injection analysis (FIA) is widely adopted in analytical chemistry due characteristics such as low sample consumption, repeatability of results, high throughput and versatility [35]. The individually driven multiple gold electrodes were tested as amperometric sensors under flow conditions. The potential of the working electrode was held constant at 0.400 V versus Ag/AgCl and the amperometric response for each working electrode was measured. Fig. 4 shows the amperometric response for 3-μl injections of $1.17 \times 10^{-3}$ mol l$^{-1}$ $K_4Fe(CN)_6$ in 0.2 mol l$^{-1}$ KCl at 100 μl min$^{-1}$ for the microfluidic cell with three toner layers. The FIA-amperometric responses for the microfluidic cells with thin-layer channels that are 13 or 19 μm deep revealed similar results irrespective of the position of the electrodes. This is because the chosen potential of 0.400 V is sufficiently positive to record currents determined by mass transport in all cases, including the configurations that presented some *iR* potential drop. Repeatability of peak heights for any electrode in Fig. 4, expressed as the relative standard deviation, RSD, falls between 0.8 and 1.5%, a quite acceptable value for 3.5 nmol of injected analyte. Comparison of the average peak height of the four electrodes renders a RSD 4.3%, demonstrating that there is little variation in the geometrical area of the electrodes of the microfluidic cell produced by the proposed technique.

### 3.3. Comparison of the use of external and internal auxiliary electrode for interdigitated working electrodes under flow operation

In Fig. 5, a comparison of the amperometric response for three setups, all in the *R*/*E*/*A* configuration, is presented: (A) one band electrode; (B) an array of four band electrodes with an external auxiliary electrode (Fig. 1C); (C) an interdigitated array of two combs with four electrodes, one acting as working electrode and one as auxiliary electrode. For 10-μl injections of $K_4Fe(CN)_6$ at a flow rate of 150 μl min$^{-1}$ and 0.400 V versus Ag/AgCl, by switching from condition A to B, a current growth of approximately four times was observed. The extra increase of 15% from B to C can be explained on basis of the contribution of *redox cycling* process. A fraction of the ferrocyanide oxidized at one electrode is reduced at the next (auxiliary) one and made available again for the forthcoming electrode while the analyte flows through the cell, thus reducing the depletion. An increase in the relative contribution of *redox cycling* to the measured current was observed with the decrease of the flow rate, e.g., at 10 μl min$^{-1}$, the difference in peak height from B to C amounted 40%. It is well known that another way to increase redox cycling is to use a larger number of smaller and much more closely spaced IDAs [14]. With the electrode preparation process used here, the minimum size of bands and gaps can be reduced to 100 and 50 μm, respectively [26], one order of magnitude less than the 1.0 mm bands and gaps chosen for the microcells shown in Fig. 1 and more suitable for effective exploration of the *redox cycling* process.

The observed RSD for the current peaks measurements in Fig. 5 were just 2.2% ($n = 11$) for one electrode band, 1.1% ($n = 12$) for a comb with four bands' electrode using internal auxiliary electrode and 1.1% ($n = 9$) for same comb using the external auxiliary electrode, respectively.

### 3.4. Biamperometric detection

Biamperometric detection in flow-injection analysis (FIA) is an attractive alternative because it requires simpler instrumentation (no potentiostat and no reference electrode needed) and it presents increased selectivity for reversible redox couples [36]. In recent years, some applications of IDA to micro-

analytical determinations have appeared in the literature [37], but combination of IDA with FIA seems still unexplored. The biamperometric signals for IDA gold electrodes with a constant potential difference of 0.100 V between the combs are shown in Fig. 5. For repetitive injections of 10-μl of a $1.17 \times 10^{-4}$ mol $l^{-1}$ $K_4Fe(CN)_6$ (0.2 mol $l^{-1}$ KCl), at 150 μl $min^{-1}$, and the sampling frequency was about 48 $h^{-1}$, an average peak current of $0.91 \pm 0.02$ μA was obtained, corresponding to an RSD of just 2.2% ($n = 19$). Detection limit ($3\sigma$) for $K_4Fe(CN)_6$ was estimated to be $3.1 \times 10^{-6}$ mol $l^{-1}$.

## 4. Conclusion

The results shown in this work have demonstrated the great potential of the proposed individually driven interdigitated gold electrodes and IDA gold electrodes in microfluidic cells of very simple construction. The easiness of construction of microfluidic devices by the adopted technology, associated to the reduced cost, propitiates the fast development of prototypes. The materials of the microfluidic cells are chemically resistant to most aqueous solutions used in electroanalysis and the cells are long lasting, in excess of 30 days. The cell resists harsh manipulation due to the epoxy-glue reinforced edges of the (smaller) upper polycarbonate slice. Detachment of the toner from one of the two polycarbonate slices has been observed by pressure buildup at "high" flow rates (>200 μl $min^{-1}$), with the increased internal dead volume causing sluggish amperometric response. Using $K_4Fe(CN)_6$ as model system, the electrochemical response for individually driven interdigitated gold electrodes was evaluated and explained as a combination of the influences of the placement of the reference and auxiliary electrodes against the working electrodes and the thickness of the electrolyte layer. The detection limit for two different configurations of the working electrodes ($E_i/R/A$ and $R/E_i/A$) and operation modes (amperometric or biamperometric) are similar and estimated to be approximately $3 \times 10^{-6}$ mol $l^{-1}$ for $K_4Fe(CN)_6$.

The area reproducibility of the electrodes of a chip is better then 5% and the production process is certainly the easiest, fastest and cheapest presently available to obtain interdigitated gold electrodes and microfluidic cells in the analytical chemistry laboratory. Although photolithography, a more demanding and laborious processes, can produce much smaller electrodes with sub-micrometric accuracy, this is not necessary for most electroanalytical applications, as exemplified here; even the benefits of some current amplification by *redox cycling* were obtained for FIA with the microfluidic cell comprising IDA under amperometric or biamperometric operation. Flow management and solution cleanliness (in terms of suspended particles) required for FIA is also easier to attain in the low microliter than in the low nanoliter range. Many new applications can be envisioned for the microfluidic cells, by exploring not only cell and electrode geometries and configurations but also electrode modification and the potentiality to perform spectroelectrochemical measurements.

## Acknowledgements

Authors are thankful to Fundação de Amparo à pesquisa do Estado de São Paulo (FAPESP) for financial support and to Conselho Nacional do Desenvolvimento Científico e Tecnológico (CNPq) for a grant. The assistance of Mr. Fernando S. Lopes in writing the software for the potentiostat was much appreciated.

## References

[1] J. Wang, Trends in Anal. Chem. 21 (2002) 226.
[2] J. Wang, M. Pumera, M.P. Chatrathi, A. Escarpa, R. Konrad, A. Griebel, W. Dorner, H. Lowe, Electrophoresis 23 (2002) 596.
[3] J. Wang, R. Polsky, B. Tian, M.P. Chatrathi, Anal. Chem. 72 (2000) 5285.
[4] R.G. Compton, B.A. Coles, J.J. Gooding, A.C. Fisher, T.I. Cox, J. Phys. Chem. 98 (1994) 2446.
[5] O. Niwa, H. Tabei, B.P. Solomon, F.M. Xie, P.T. Kissinger, J. Chromatogr. B 670 (1995) 21.
[6] J. Wang, Talanta 56 (2002) 223.
[7] C. Amatore, M. Belotti, Y. Chen, E. Roy, C. Sella, L. Thouin, J. Electroanal. Chem. 573 (2004) 333.
[8] N.S. Lawrence, E.L. Beckett, J. Davis, R.G. Compton, Anal. Biochem. 303 (2002) 1.
[9] D.A. Roston, R.E. Shoup, P.T. Kissinger, Anal. Chem. 54 (1982) 1417.
[10] K. Reimer, C. Köhler, T. Lisec, U. Schnakenberg, G. Fuhr, R. Hintsche, B. Wagner, Sens. Actuators A 46–47 (1995) 66.
[11] R.S. Martin, A.J. Gawron, S.M. Lunte, C.S. Henry, Anal. Chem. 72 (2000) 3196.
[12] M. Zhao, D.B. Hibbert, J.J. Gooding, Anal. Chem. 75 (2003) 593.
[13] A.J. Gawron, R.S. Martin, S.M. Lunte, Electrophoresis 22 (2001) 242.
[14] M. Morita, O. Niwa, T. Horiuchi, Electrochim. Acta 42 (1997) 3177.
[15] R. Kurita, H. Tabei, Z. Liu, T. Horiuchi, O. Niwa, Sens. Actuators B 71 (2000) 82.
[16] P. Jin, A. Yamaguchi, F.A. Oi, S. Matsuo, J. Tan, H. Misawa, Anal. Sci. 17 (2001) 841.
[17] P. Tomcík, M. Krajcíková, D. Bustin, Talanta 55 (2001) 1065.
[18] K. Toda, Y. Komatsu, S. Oguni, S. Hashiguchi, I. Sanemasa, Anal. Sci. 15 (1999) 87.
[19] K. Hayashi, Y. Iwasaki, R. Kurita, K. Sunagawa, O. Niwa, Electrochem. Commun. 5 (2003) 1037.
[20] K. Aoki, M. Morita, O. Niwa, H. Tabei, J. Electroanal. Chem. 256 (1988) 269.
[21] M.G. Sullivan, H. Utomo, P.J. Fagan, M.D. Ward, Anal. Chem. 71 (1999) 4369.
[22] M. Paeschke, U. Wollenberger, T. Lisec, U. Schnakenberg, R. Hintsche, Sens. Actuators B 26 (1995) 394.
[23] A.E. Cohen, R.R. Kunz, Sens. Actuators B 62 (2000) 23.
[24] K. Ueno, M. Hayashida, J.-Y. Ye, H. Misawa, Electrochem. Commun. 7 (2005) 161.
[25] C.L. Lago, H.D.T. Silva, C.A. Neves, J.G. Brito-Neto, J.A.F. Silva, Anal. Chem. 75 (2003) 3853.
[26] D. Daniel, I.G.R. Gutz, Electrochem. Commun. 5 (2003) 782.
[27] T.R.L.C. Paixão, R.C. Matos, M. Bertotti, Electrochim. Acta 48 (2003) 691.
[28] J.J. Pedrotti, L. Angnes, I.G.R. Gutz, Electroanalysis 8 (1996) 673.
[29] J.S. Rossier, M.A. Roberts, R. Ferrigno, H.H. Gorault, Anal. Chem. 71 (1999) 4294.
[30] K. Ueno, H.B. Kim, N. Kitamura, Anal. Chem. 75 (2003) 2086.
[31] J.C. Myland, K.B. Oldham, Anal. Chem. 72 (2000) 3972.
[32] A.J. Bard, L.R. Faulkner, Electrochemical Methods: Fundamentals and Applications, 2nd ed., Wiley, New York, 2001, p. 409.

[33] T. Ito, K. Maruyama, K. Sobue, S. Ohya, O. Niwa, K. Suzuki, Electroanalysis 24 (2004) 2035.
[34] A.T. Hubbard, J. Electroanal. Chem. 22 (1969) 165.
[35] J. Ruzicka, E.H. Hansen, Flow Injection Analysis, 2nd ed., Wiley, New York, 1988.
[36] M.C. Icardo, D.G. Romero, J.V.G. Mateo, J.M. Calatayud, Anal. Chim. Acta 407 (2000) 187.
[37] P. Tomčík, L. Mrafková, D. Bustin, Microchim. Acta 141 (2003) 69.